JOURNAL OF NEUROTRAUMA 28:2307–2318 (November 2011)

DOI: 10.1089/neu.2011.1718

Blast-Induced Color Change in Photonic Crystals Corresponds with Brain Pathology

D. Kacy Cullen,[1] Kevin D. Browne,[1] Yongan Xu,[2] Saleena Adeeb,[3] John A. Wolf,[1] Richard M. McCarron,[3] Shu Yang,[2] Mikulas Chavko,[3] and Douglas H. Smith[1]

Abstract

A high incidence of blast exposure is a 21st century reality in counter-insurgency warfare. However, thresholds for closed-head blast-induced traumatic brain injury (bTBI) remain unknown. Moreover, without objective information about relative blast exposure, warfighters with bTBI may not receive appropriate medical care and may remain in harm's way. Accordingly, we have engineered a blast injury dosimeter (BID) using a photonic crystalline material that changes color following blast exposure. The photonic crystals are fabricated using SU-8 via multi-beam interference laser lithography. The final BID is similar in appearance to an array of small colored stickers that may be affixed to uniforms or helmets in multiple locations. Although durable under normal conditions, the photonic crystalline micro- and nano-structure are precisely altered by blast to create a color change. These BIDs were evaluated using a rat model of bTBI, for which blast shockwave exposure was generated via a compressed air-driven shock tube. With prototype BID arrays affixed to the animals, we found that BID color changes corresponded with subtle brain pathologies, including neuronal degeneration and reactive astrocytosis. These subtle changes were most notable in the dentate gyrus of the hippocampus, cerebral cortex, and cerebellum. These data demonstrate the feasibility of using a materials-based, power-free colorimetric BID as the first self-contained blast sensor calibrated to correspond with brain pathology.

Key words: blast exposure; blast injury detection; blast injury dosimeter; blast neuropathology; blast sensor; mild traumatic brain injury; nanomaterial

Introduction

Although blast-induced traumatic brain injury (bTBI) is considered the signature injury of the current wars in Iraq and Afghanistan, little is known about the minimum thresholds of blast exposure required to induce brain pathology. As such, acute mild bTBI may be missed in many warfighters, placing them at risk of repeat exposures and potential exacerbation of their injury if they return to battle. The high incidence of bTBI observed in current conflicts appears to be a 21st-century phenomenon, due in part to the counter-insurgency nature and increased use of improvised explosive devices (IEDs) in current wars (Hoge et al., 2008; Okie, 2005; Phillips and Richmond, 1991; Warden, 2006). In addition, while improvements in body armor protect many warfighters from otherwise lethal blast injuries to air-filled organs, this likely increases the number of soldiers surviving with bTBI. Also, there is substantial debate regarding the prevalence of bTBI, with the highest estimates at 15–20% of the warfighters (over 300,000 soldiers) having served in Iraq or Afghanistan (Hoge et al., 2009; Tanielian and Jaycox, 2008; Wojcik et al., 2010). However, there may be an alarmingly low detection rate for closed-head mild bTBI, with many diagnoses not made until months after injury (Hoge et al., 2009; Van Boven et al., 2009).

Accordingly, there is great interest in deploying technologies to record an individual's blast exposure in combat situations. For instance, helmet-mounted pressure transducers are being developed to record blast exposure, and are currently being tested in limited deployment. However, to date such systems have been cumbersome, require a power supply, and may not be useful in extreme combat conditions. As such, we have developed a wearable and durable materials-based dosimeter for the detection of blast exposure based on a simple color change (Fig. 1A). This blast injury dosimeter (BID) consists of 3D microstructures comprised of layered

[1]Center for Brain Injury and Repair, Department of Neurosurgery, and [2]Department of Materials Science and Engineering, University of Pennsylvania, Philadelphia, Pennsylvania.
[3]Trauma and Resuscitative Medicine Department, Naval Medical Research Center, Silver Spring, Maryland.

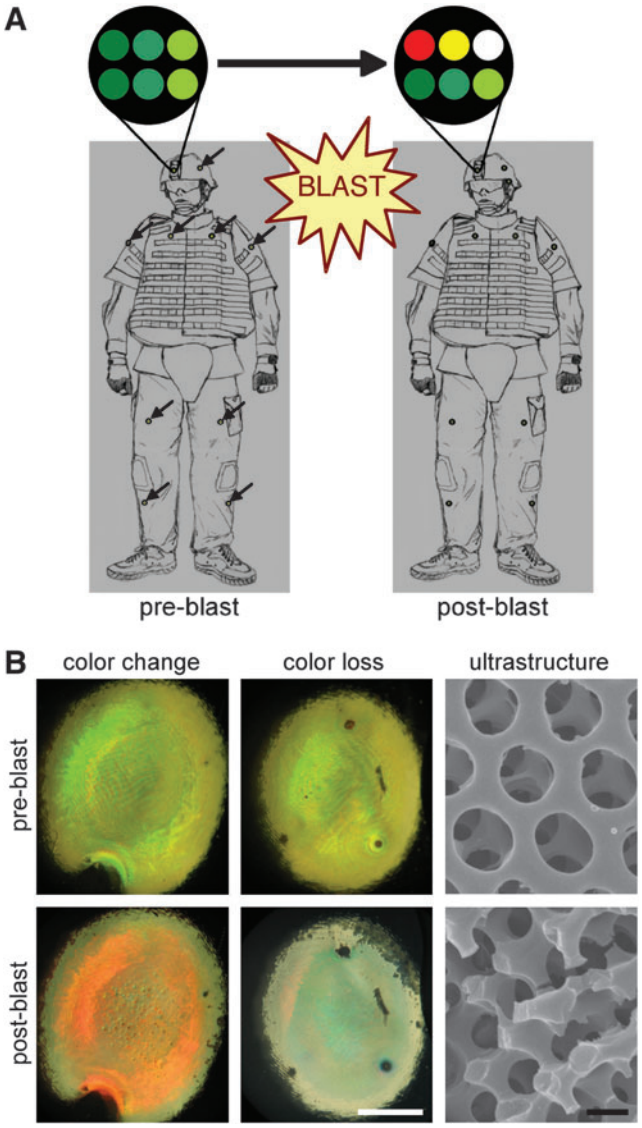

FIG. 1. Blast injury dosimeter (BID) concept and function. (**A**) BID arrays may be affixed to warfighter uniforms in multiple locations. These arrays consist of multiple engineered photonic crystalline microstructures, the colorimetric properties of which are a result of the nano-scale structure, creating so-called "structural color." (**B**) We have previously demonstrated that blast exposure precisely disrupts the structure at the nano- and micro-scales, creating color change and loss, respectively (color change/loss scale bar = 1 mm; SEM scale bar = 500 nm). These properties make our photonic crystalline arrays ideal to serve as a colorimetric blast injury dosimeter. Schematic adapted from Cullen and associates (2011; SEM, scanning electron microscope).

photonic crystals (6 μm total thickness) created from SU-8, a commercially available photoresist polymer, using multi-beam interference lithography (MBIL; Campbell et al., 2000; Miklyaev et al., 2003; Moon and Yang, 2005; Yang et al., 2002; Xu et al., 2008). In photonic crystals, the color is a consequence of the nano-structure rather than being an inherent property of the chemical composition. In these cases, color has a physical origin due to the diffraction or interference of light, resulting in so-called "structural color." This basic technology mimics the photonic crystalline structure responsible for the brilliant colors commonly seen in the wings of some birds (e.g., peacock) and butterflies (e.g., Morpho; Ghiradella et al., 1972; Kinoshita and Yoshioka, 2005; Li et al., 2005; Noh et al., 2010; Vukusic and Sambles, 2003; Zi et al., 2003). Blast shockwave exposure of sufficient intensity disrupts the 3D ultrastructure in a precise fashion; when the structure is disrupted, the color is changed or lost (Fig. 1B). Moreover, the degree of nano- and micro-scale structural damage, and hence color change/loss, may be tuned based on shockwave characteristics supra-threshold for bTBI. Similar in concept to a radiation badge, these BID arrays may be fabricated to denote bTBI risk based on a single exposure or to measure cumulative exposure.

In proof-of-concept studies, we demonstrated color change and loss in these photonic crystalline nanostructures due to blast exposure (Cullen et al., 2011). However, the blast levels tested would likely cause severe, extensive injuries or death in humans, with peak overpressures ranging from approximately 410–1090 kPa, and thus would not require dosimetry. Therefore, our objective was to demonstrate the efficacy of this sensor technology, based on readily observed color change and/or color loss, at survivable blast levels inducing brain pathology. We utilized a model of bTBI in the rat in which blast shock-wave exposure was generated via a compressed air-driven shocktube (Fig. 2). BID arrays were affixed to rats prior to blast shockwave in order to examine the capability of the photonic crystalline BID to undergo color changes in concert with overt or subtle neuropathology (Fig. 2D and E). We found that BID color change corresponded with neuronal degeneration and reactive astrocytosis. The most vulnerable regions of the brain were the dentate gyrus of the hippocampus, aspects of the cerebral cortex, and the cerebellum. Importantly, this work establishes an experimental framework by which this technology can be used to measure and determine minimum blast exposure levels for single or cumulative injuries in rats or higher-order species.

Methods

Photonic crystal fabrication

Diamond-like photonic crystals consisting of periodic arrangement of polymer and air voids were fabricated from the negative photoresist SU-8 by MBIL (Xu et al., 2008). Briefly, SU-8 film was exposed to four umbrella-like visible laser beams split from one coherent laser source ($\lambda = 532$ nm, power diode-pumped Nd:YVO_4 laser). The central beam was circularly polarized and incident perpendicularly to the photoresist film. The other three beams were polarized linearly in a plane formed by the wave vectors of the central beam and surrounding beam. The wave vector of each beam was $k_0 = \partial/\alpha[333]$, $k_1 = \partial/\alpha[511]$, $k_2 = \partial/\alpha[151]$, and $k_3 = \partial/\alpha[115]$, respectively. The polarization vectors of beam 1, 2, and 3 were $e_1 = [-0.2720.6800.680]$, $e_2 = [0.680\text{-}0.272\ 0.680]$, and $e_3 = [0.6800.680\ -0.272]$, respectively. The intensity ratio was 1.8:1:1:1. The circular polarization of the central beam distributes the intensity equally to the surrounding beams.

The photoresist was prepared by mixing Epon SU-8 pellets and 2.0 wt % Irgacure 261 (Ciba Specialty Chemicals, Basel, Switzerland) as visible photoinitiators in γ-butyrolactone (Sigma-Aldrich, St. Louis, MO) to form 58-wt% solution.

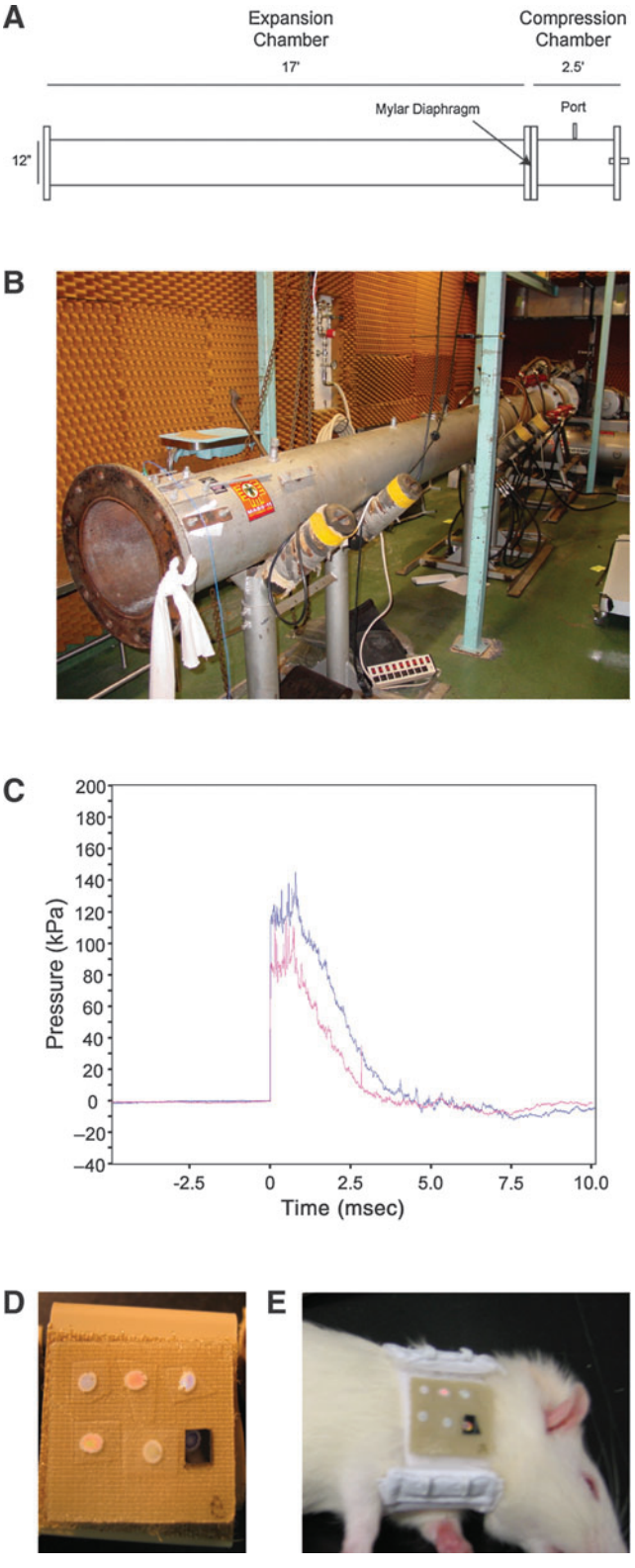

FIG. 2. Experimental shocktube and blast injury dosimeter (BID) arrays. (**A**) Schematic and (**B**) photograph of the compressed air-driven shocktube. (**C**) Example of pressure changes with respect to time generated by the shock tube. (**D**) Arrays of BIDs with various structural and colorimetric properties were tested. (**E**) Arrays were affixed to rats immediately adjacent (caudal) to their heads prior to lateral blast exposure (from the right side).

Substrates were rigid silicon or flexible aclar membranes (SPI Supplies, West Chester, PA). To ensure good adhesion with the SU-8 film, the substrate was cleaned by ultrasonication in isopropanol and acetone, followed by oxygen plasma. The photoresist solution was spin-coated on the substrate at 2000 rpm for 30 sec, followed by a pre-exposure bake at 65°C for 3 min and 95°C for 40 min, resulting in a film thickness of $\sim 6\,\mu$m. The film was exposed to the superimposed interference beams (laser output of 1 W) for 1–2 sec. After a post-exposure bake at 65°C for 2–4 min and 95°C for 2–4 min, the exposed film was developed in propylene glycol monomethyl ether acetate (Sigma-Aldrich) to remove unexposed or weakly exposed films, resulting in 3D microporous structures. To prevent the pattern collapse of the 3D porous film during air-drying, the film was dried using a supercritical CO_2 dryer (SAMDRI®-PVT-3D; tousimis, Rockville, MD) after development.

Each BID consisted of a photonic crystalline microstructure, appearing like a simple colored dot a few millimeters in diameter, with a total thickness of 6 μm (typically 6 crystalline layers, each 1 μm thick). The BIDs are chemically and thermally (up to 300°C) stable, rendering them extremely durable under motion, moisture, and temperature conditions associated with extremely hot or cold combat environments. Multiple BIDs were combined onto a thin flexible sheet ($<1\,cm^2$) to create a BID array, resembling a matrix of small colored stickers.

Shocktube testing

We evaluated the structural/colorimetric alterations of BID arrays following exposure to surrogate blast conditions. Here we utilized an established model of bTBI using a compressed air-driven shocktube with rats. This device has been used extensively to study various aspects of blast overpressure and blast-induced injury (Chavko et al., 2006,2007,2008,2009; Elsayed and Gorbunov, 2003,2007; Elsayed et al., 1997; Gorbunov et al., 1997, Long et al., 2009). The shocktube is cylindrical, 1 foot in diameter with a 2.5-foot compression chamber and a 17-foot expansion chamber separated by a Mylar sheet of specified thickness (Fig. 2A and B). To generate blast shockwave, the compression chamber was pressurized, resulting in Mylar rupture at a critical pressure level that caused a pressure wave to propagate along the expansion chamber. The Mylar thickness, and hence rupture pressure, determined the blast pressure wave characteristics and magnitude (Fig. 2C).

Imaging of photonic crystalline microstructures

Light images were taken for each BID before and after surrogate blast or control (sham) conditions. Images were acquired by a digital camera mounted on a stereoscope at 10× magnification. Scanning electron microscopy (SEM) ultrastructural analysis was performed using a Strata DB235 Focused Ion Beam system (FEI) at an e-beam voltage of 5 kV. The samples were sputter-coated with gold (<10 nm) prior to SEM analysis.

Rat model of bTBI and histopathology

All procedures involving animals were approved by the WRAIR/NMRC Institutional Animal Care and Use Committee, and followed the National Institutes of Health (NIH) "Guide for the Care and Use of Laboratory Animals" (NIH

publications no. 80-23; revised 1996). Sprague-Dawley rats (250–300 g) were anesthetized using isoflurane, placed in a basket within the shocktube (approximately 2 feet into the expansion chamber), and exposed laterally (right side) to a blast wave at a peak overpressure of approximately 120 or 140 kPa, causing sustained overpressure lasting 3–4 msec ($n=18$ rats), or sham (non-exposed) conditions ($n=4$ rats). BID arrays were affixed to a subset of the rats prior to blast shockwave exposure (Fig. 2D and E). Neuropathology was assessed in the same animals equipped with BID arrays, as well as other animals exposed to identical blast conditions but not wearing BID arrays.

The animals were euthanized at 3, 24, and 48 h post-injury ($n=3$ per blast level per time point) by transcardial perfusion with heparinized saline and 4% paraformaldehyde. The brains were harvested and photographed for gross pathology. Brains were blocked (2-mm sections), embedded in paraffin, sectioned (7 μm), and stained with hematoxylin and eosin (H&E) and cresyl violet (CV) to evaluate neuronal degeneration and cell loss, respectively. Gallyas silver staining with neutral red counter-stain was performed to assess neuronal somatic and axonal changes. The density of degenerating neurons was semi-quantitatively assessed in coronal sections (at 1-mm intervals rostral to caudal). Briefly, one section from each of 6 regions within the brain (+1 mm to the bregma, the bregma to −1, −2.5 to −3.5, −4.5 to −5.5, −6 to −7, and −7.5 to −8.5) was evaluated by quantifying density profiles: low-density profiles consisted of less than approximately 25 shrunken, darkly-stained, triangular-shaped neurons per 1.2 mm^2 field (10× objective); moderate-density profiles had between 26 and 100 neurons; and high-density profiles had greater than 100 neurons.

Immunohistochemistry for astrogliosis was performed using a rabbit anti-glial fibrillary acidic protein (GFAP) antibody (AB5408, 1:750; Millipore Corp., Billerica, MA). Immunohistochemistry for axonal pathology was carried out on separate sections using a monoclonal antibody against neurofilament 200 (NF200, clone N52, 1:200; Sigma-Aldrich), and a monoclonal antibody against amyloid precursor protein (APP, clone 22c11, 1:60,000; Millipore). For GFAP staining, the sections were deparaffined and rehydrated, and endogenous peroxidase activity was blocked using 5% hydrogen peroxide in methanol. The slides were rinsed with distilled water, microwaved in PBS for antigen retrieval, blocked in 2% normal horse serum, and incubated in primary antibody overnight at 4°C. The slides were then rinsed, washed several times in PBS, and incubated in donkey anti-rabbit HRP-conjugated secondary antibody for 1 h (1:500; Jackson ImmunoResearch Labs, West Grove, PA). After washing in distilled water, tissue was counterstained with Harris hematoxylin, dehydrated, and cover-slipped. Sections for NF200 staining were processed identically, except primary antibody incubation occurred at room temperature, and the following day the slides were washed in PBS, and donkey anti-mouse horseradish peroxidase (Jackson ImmunoResearch Labs) was applied. For both GFAP and NF200, the sections were rinsed, washed in PBS, and incubated in 3,3′-diaminobenzidine (DAB; Vector Labs, Burlingame, CA) for visualization. For APP staining, slides were deparaffinized, rehydrated, and endogenous peroxidase activity was blocked as described above. Epitope retrieval was achieved using a pressure cooker. The slides were then blocked using the Vector Elite Universal ABC kit and the primary applied and left to incubate overnight at 4°C. The following day, the slides were washed and the secondary was applied according the Vector Elite kit instructions. Visualization was achieved using DAB.

Microscopic analyses and photomicrograph acquisition utilized either a Nikon Eclipse 600 microscope equipped with a DS-Ri1 camera (Nikon Instruments, Inc., Melville, NY), or a SPOT RT3 slider camera (Diagnostic Instruments, Inc., Sterling Heights, MI).

Results

Gross brain pathological changes

Anesthetized rats were exposed to sham conditions or lateral blast shockwave (right side) at peak overpressures of 120 or 140 kPa. There was no mortality associated with the blast exposure, and the animals were euthanized at 3, 24, and 48 hr post-injury. Subdural hematomas were found in a subset of the animals subjected to blast shockwave, and when observed were located over the cerebral cortex or cerebellum tentori with no obvious differences in hemisphere location. The size of the ventricles did not appear to change following injury. There were no obvious signs of edema. Residual blood from the subdural bleeds was present but not grossly visible within the parenchyma of the brain. Overall, these gross pathological changes were found equally between animals subjected to 120 and 140 kPa peak overpressure blast.

Histopathological findings

There were overt histopathological changes in animals exposed to blast shockwave compared to sham animals (described in detail below); however, there were no differences between animals subjected to 120 versus 140 kPa blast, so these groups were combined for our analysis of blast-induced neuropathology. Routine microscopic examination confirmed the presence of blood within the ventricles in approximately 30% of the injured animals, with micro-clots or micro-hemorrhages observed in fewer than 20% of injured animals. Histopathological analysis demonstrated neuronal degeneration in the injured group, with affected neurons appearing shrunken, irregularly shaped, and darkly stained. Surprisingly, these pyknotic neurons were observed as early as 3 h post-injury, and persisted up to 48 h post-injury (Fig. 3). The extent of pyknotic profiles varied based on density and location between individual animals and across time points. Specifically, in sham animals there were an average of 8 low-density profiles (defined as <25 pyknotic neurons per profile) per brain. However, at 3 h post-blast, the average number of profiles per brain was 10.5 low-density, 12.2 moderate-density (26–100 pyknotic neurons), and 7.0 high-density (>100 pyknotic neurons; Table 1). At 24 and 48 h, the number of moderate- and high-density profiles remained virtually unchanged; however, there were over 40% more low-density profiles at 48 h compared to 3 h, and over 50% more at 48 h compared to 24 h, indicating ongoing degeneration. Notably, there were obviously more pyknotic neurons (moderate- and high-density profiles) on the right side of the brain (towards the blast) than the left. Pyknotic neurons were observed primarily in the cerebral cortex, and to a lesser extent in the hippocampus, primarily in the medial portion of the dentate gyrus of the dorsal hippocampus and the dentate gyrus/CA3

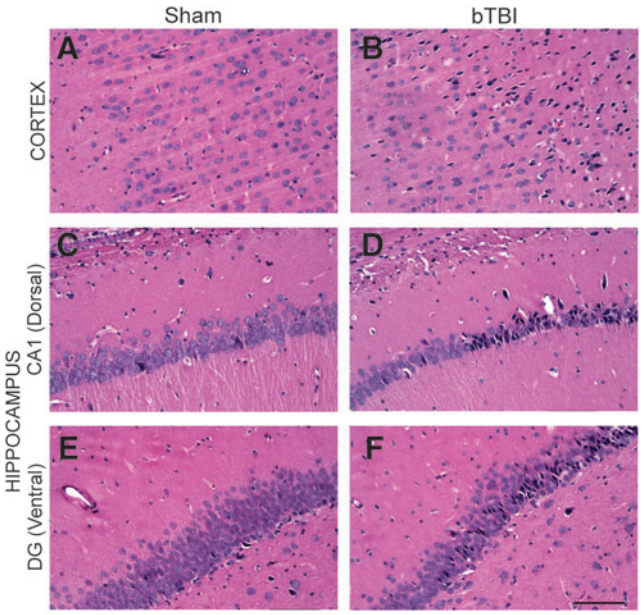

FIG. 3. Blast-induced neuronal degeneration. Hematoxylin and eosin (H&E) staining demonstrated pyknotic neurons following lateral (right) blast exposure. Pyknotic neurons, appearing dark and irregularly shaped, indicate degeneration. In the cerebral cortex (**A** and **B**) and hippocampal formation (**C** and **F**), a wide range of degenerative profiles (based on density and location) was observed at 3, 24, and 48 h post-blast compared to sham animals. In particular, multiple degenerative profiles were observed in (**B**) the cerebral cortex, (**D**) the CA1 region (dorsal), and (**F**) the medial portion of the dentate gyrus (DG, ventral; scale bar = 100 μm; bTBI, blast-induced traumatic brain injury).

region of the ventral hippocampus (Fig. 4). However, no overt tissue loss or shrinkage of the hippocampi was observed after blast exposure within the time points examined. Degenerating neurons were not observed in the cerebellum at these time points. Cresyl violet staining confirmed the presence of affected cells in the same regions observed with H&E staining.

Blast shockwave exposure also induced reactive astrogliosis, demonstrated both morphologically and by immunoreactivity to GFAP. Specifically, astrocytes appeared hypertrophied with more intense GFAP staining after blast exposure. While astrocyte reactivity was observed throughout the brains following blast shockwave, it appeared most pronounced in the cerebellum throughout the molecular layers (Fig. 5). In the cerebrum, astrocyte reactivity was significantly increased (versus sham animals), most notably in proximity to the cingulum, the interface of the cortex and the corpus callosum, and along the interface of the cortex and external capsule. Similarly, hypertrophied astrocytes were observed in the dentate gyrus of the hippocampal formation.

Table 1. Density Profiles of Degenerating Neurons

		Density profiles		
		Low (<25 pyknotic neurons)	*Moderate (26–100 pyknotic neurons)*	*High (>100 pyknotic neurons)*
Time post-blast	3 h	10.5	12.2	7
	24 h	7.6	13.2	5.6
	48 h	14.8	13.6	5.6

Axonal pathology was assessed using antibodies to NF200 and APP, abundant intra-axonal proteins that accumulate due to trauma-induced transport interruptions, a hallmark pathology of diffuse axonal injury (DAI; Chen et al., 1999, Smith et al., 1999,2003). We analyzed throughout the brain, but specific focus was given to the corpus callosum and the internal and external capsules, where we expected the most prominent axonal pathology to be located. This analysis revealed no overt evidence of diffuse axonal bulbs or axonal swellings. Additionally, we used Gallyas silver staining to assess neuronal degeneration and to further probe for potential axonal pathology. This analysis focused on the cerebral cortex, the corpus callosum, the internal and external capsules, and the hippocampal formation, including perforant path axons. Following blast shockwave, neuronal degeneration was observed in the cortex and hippocampus, confirming results attained by H&E staining. Many layer IV neurons in the cortex appeared dark and irregularly shaped, suggesting early degeneration; however, the quantity and distribution of these degenerating neurons did not change over the time points evaluated (Fig. 6). Again, prominent axonal pathology was not observed, as axons in the corpus callosum and perforant path appeared unremarkable.

Corresponding BID colorimetric change and neuropathology following blast shockwave exposure

BID arrays were affixed to rats prior to blast shockwave exposure. In all cases, the arrays remained on the rats during blast exposure and the photonic crystal dots remained adhered to the substrate, which was not overtly damaged. Corresponding with pathological changes, a subset of the BIDs affixed to the animals exposed to blast shockwave demonstrated overt color changes (Fig. 7A and B). In particular, over 80% of the BIDs tested in this study changed color following blast overpressure of 140 kPa, but less than 60% of the BIDs changed color following 120 kPa exposure. In addition, by design, other BIDs did not exhibit a color change at either blast level due to higher ultrastructural failure thresholds (Fig. 7C). These findings establish the use of arrays consisting of BIDs with various thresholds to establish an accurate range of blast shockwave exposure levels. These observations also underscore that the photonic crystals are specifically and precisely altered by blast shockwave.

Discussion

There has been a critical unmet need to measure an individual's blast exposure to identify potential bTBI. Without this information, clinical management of exposed individuals may be insufficient. Using a rat model of bTBI, we have demonstrated the capability of the photonic crystalline BID to undergo color changes following sub-lethal blast exposure at levels inducing subtle brain pathology. We surveyed a range of neuropathologies, and found prominent neuronal degeneration in aspects of the cerebral cortex and hippocampus, and substantial reactive astrocytosis in the dentate gyrus and the cerebellum. This is first materials-based self-contained

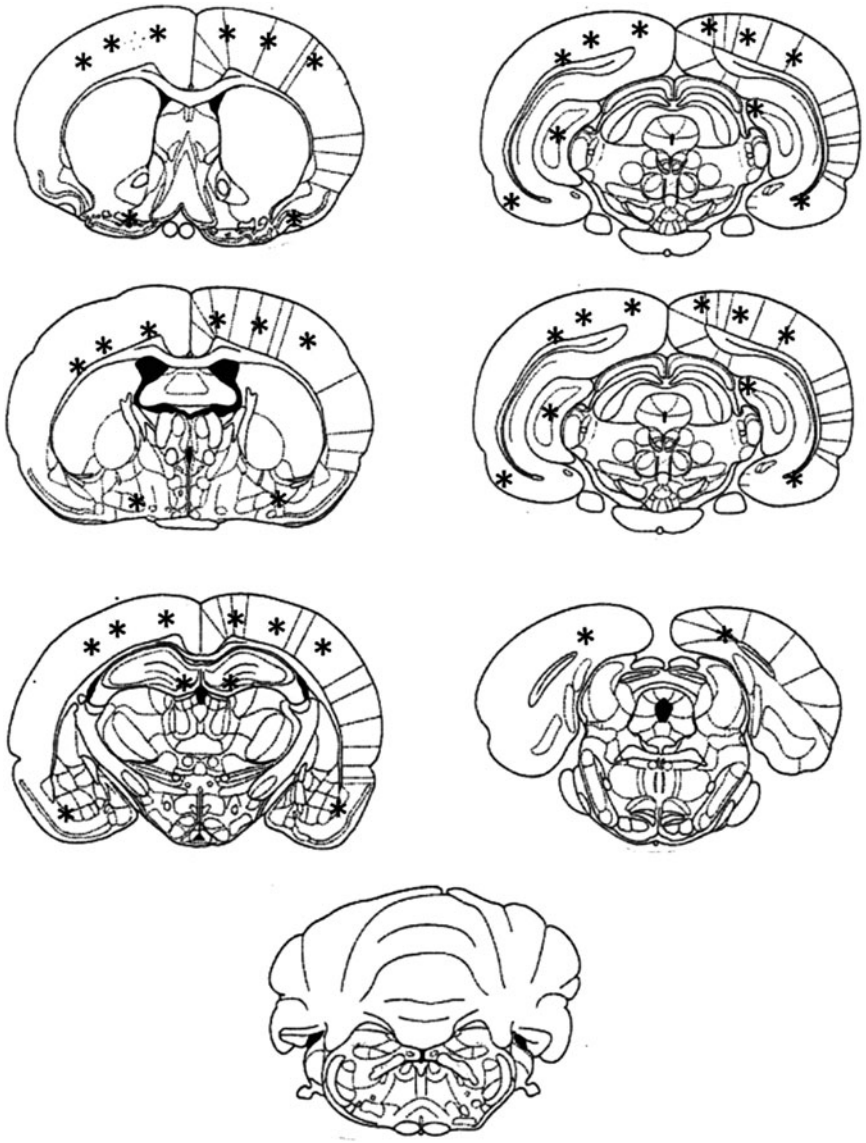

FIG. 4. Schematic diagram depicting the general regional distribution of degenerative profiles following lateral blast exposure. This schematic is a compilation independent of survival time and the density of the profiles. While not shown directly in this figure, there were more moderate- and high-density profiles observed on the right side of the brain than the left. Neuronal degeneration was primarily observed throughout the cortex, in the dorsal hippocampus in the medial portion of the dentate gyrus, and in the ventral hippocampus in the dentate gyrus/CA3 region. Note the lack of degenerating neurons in the cerebellum.

blast dosimeter capable of measuring relative blast exposure where calibration has occurred based on subtle neuropathology in animals. In consideration of its use in combat conditions, this colorimetric sensor is small, lightweight, durable, and requires no power. To signal injurious levels of blast exposure, the BID was specifically designed to undergo overt color changes that can be interpreted by the naked eye. While these data demonstrate the feasibility of this BID approach to detect potential bTBI in warfighters exposed to blast shockwave, extensive refinements remain to be performed to more precisely calibrate the color changes of the BID to denote the extent and potentially type of brain pathology occurring in humans. Importantly, this work establishes a systematic framework to blast injury dosimetry that we may apply in the future to calibrate BID array color changes with minimum single and cumulative blast exposure levels based on subtle neuropathology. In particular, this initial side-by-side neuropathological and materials characterization allows us to move forward to achieve a spectrum of color changes for a range of sub-lethal blast exposures associated with mild bTBI.

We previously established our strategy for blast injury detection based on optical changes in photonic crystals due to blast exposure (Cullen et al., 2011). The key feature of our BID is the exploitation of blast energy to induce physical/structural alterations at the nano-scale, manifested as overt color changes. Precise control of BID ultrastructure, including nano-scale physical and structural properties, determined the color properties as well as the responses to blast exposure. In

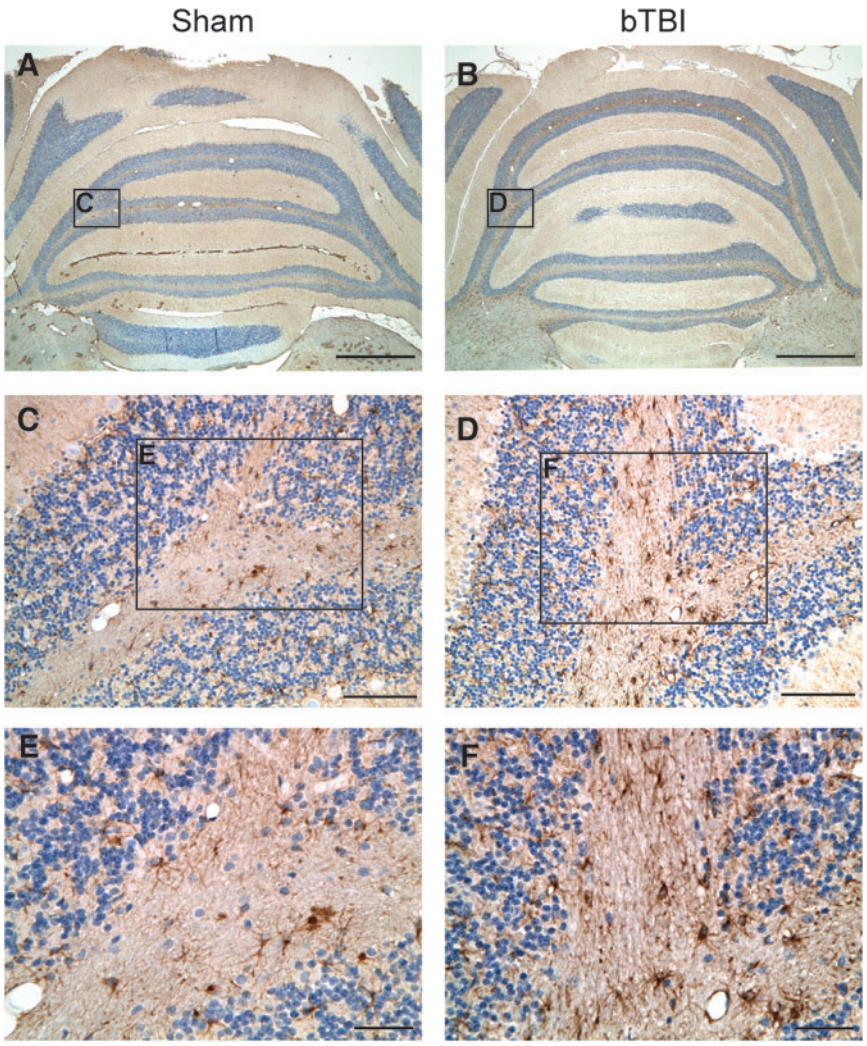

FIG. 5. Blast-induced astrogliosis. Glial fibrillary acidic protein (GFAP) staining revealed an increased astrocytic response in the cerebellum as early as 3 h post-blast. Astrocytes in the sham cerebellum (**A**, **C**, and **E**) were smaller with less intense GFAP reactivity than those in the injured cerebellum (**B**, **D**, and **F**; scale bars in **A** and **B** = 1000 μm; in **C** and **D** = 100 μM; in **E** and **F** = 20 μm; bTBI, blast-induced traumatic brain injury).

our previous work, we demonstrated BID color change and/or loss at non-survivable blast levels with peak overpressures of 410–1090 kPa. In the current work, we advanced our novel technology using a model of blast shockwave exposure with rats to demonstrate color change at survivable blast levels inducing brain pathology. These pathologies ranged from overt hematoma to more subtle, histopathologically-assessed neuronal degeneration, astrocyte reactivity, and microbleeds. By both manipulating the composition of the material and modifying the lithography technique, we may essentially tune the nano-scale physical and structural properties of the BID to fail according to differing brain pathology thresholds.

Minimum blast exposure levels capable of inducing brain pathology have yet to be established. Blast injury thresholds developed in the 20th century were primarily based on exposure levels inducing lung damage (e.g., peak incident pressure, time duration, and subject proximity to reflective surface); however, soldiers are now surviving more powerful explosions due to advances in body armor and rapid medical intervention (Martin et al., 2008). Recently, blast overpressure levels inducing brain injury have varied over several orders of magnitude, and are dependent upon the method of measuring pressure (e.g., face-on versus side-on, and sampling rate), reported parameters (e.g., reflected pressure, peak overpressure, or mean sustained overpressure), degree of exposure (e.g., whole body, head, or brain directly), and the sensitivity of particular outcomes (Cernak et al., 2001; Garman et al., 2011; Kato et al., 2007; Koliatsos et al., 2011; Moochhala et al., 2004; Saljo et al., 2008). This supports our bTBI dosimetry strategy, for which our colorimetric BID is developed in parallel with the establishment of minimum blast exposure levels to induce subtle neuropathology.

In contrast to non-blast (civilian) TBI, there has yet to be significant neuropathological characterization of bTBI in humans at any severity level. Nonetheless, it is thought that subtle pathologic changes play an important role in outcome, especially for mild bTBI. In particular, the damage in non-impact closed-head bTBI in humans is diffuse with no associated focal lesions and no pattern of anatomical deficits as evidenced with conventional brain imaging, as is the case with

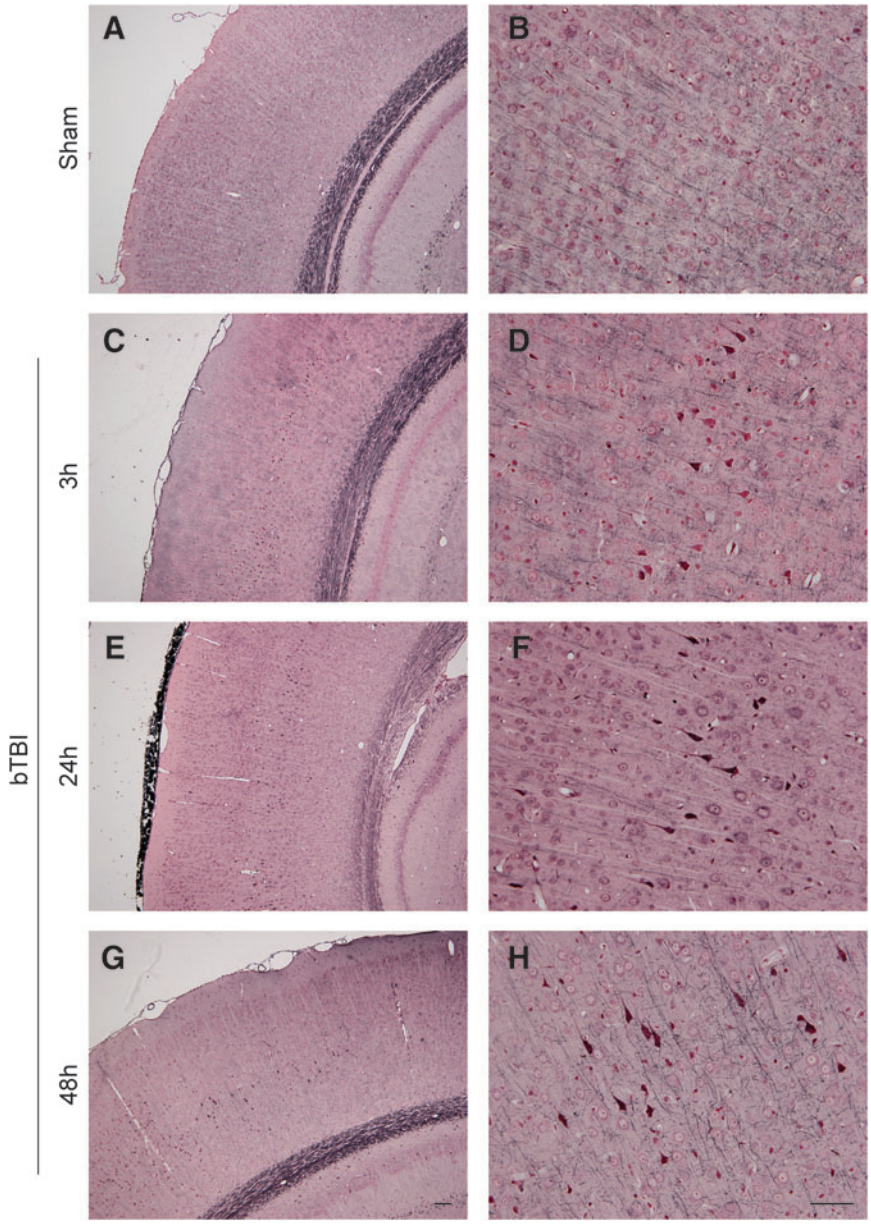

FIG. 6. Blast-induced degeneration. Silver staining demonstrated hyperintense neurons in the cerebral cortex following (**C**–**H**) blast exposure compared to (**A** and **B**) shams. In particular, degenerating neurons were observed in layer IV of the cortex at (**C** and **D**) 3 h, (**E** and **F**) 24 h, and (**G** and **H**) 48 h post-blast compared to sham animals scale bar in (**A**, **C**, **E**, and **G** = 100 μm; in **B**, **D**, **F**, and **H** = 50 μm; bTBI, blast-induced traumatic brain injury).

non-blast diffuse brain injury (Meagher et al., 2008; Mittl et al., 1994; Okie, 2005). Indeed, mild bTBI is suspected in individuals exposed to blast who exhibit persisting cognitive deficits commonly in the absence of radiological evidence of brain pathology (Elder and Cristian, 2009; Martin et al., 2008; Taber et al., 2006). As such, mild bTBI is often a diagnosis of exclusion, generally established only when in the chronic stage through extensive neurocognitive testing. However, due to this symptomatology and diffuse nature of the damage, a prominent feature of mild bTBI is believed to be DAI, although direct experimental evidence is underwhelming to date.

In animal models of bTBI, the described neuropathology has been similar to non-blast TBI, including neuronal degeneration, gliosis, demyelination, microvascular disruption, and/or transient blood–brain barrier compromise (Cernak et al., 2001; Dewitt and Prough, 2008; Kato et al., 2007; Leung et al., 2008; Long et al., 2009; Readnower et al., 2010; Saljo et al., 2000,2002). Our finding of pyknotic, degenerating neurons observed in the cerebral cortex and hippocampus is substantiated by previous reports of neuronal stress, apoptosis, and atypical accumulations of phosphorylated heavy neurofilaments (Saljo et al., 2000,2002). Notably, we did not observe significant axonal pathology at the time points observed, which, although substantiated by another study (Risling et al., 2011), is incongruent with the widely expressed belief that DAI is the prominent pathology of bTBI. However, work using the same shocktube (with the animals placed outside, affecting the blast parameters) reported widespread

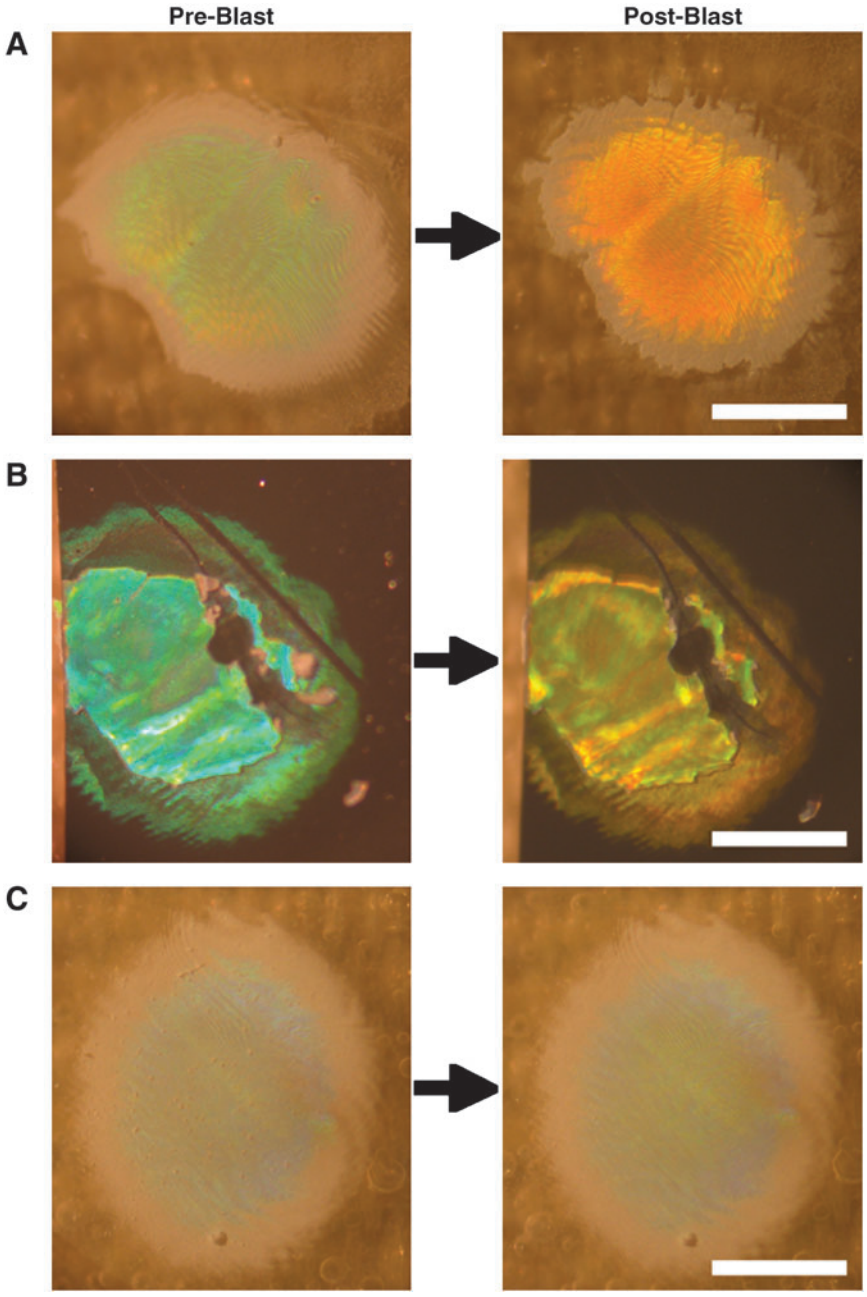

FIG. 7. Blast-induced color changes in photonic crystalline microstructures. Blast injury dosimeter (BID) arrays were affixed to rats prior to blast exposure at peak overpressure of 120 or 140 kPa. Clear blast-induced colorimetric changes were observed in individual photonic crystals on (**A**) flexible aclar substrates or (**B**) rigid silicone substrates. (**C**) Other microstructures on the same arrays required more powerful blast exposure to induce ultrastructural alterations, and did not exhibit color change. Thus, BID arrays comprised of photonic microstructures with varying blast exposure thresholds may serve as accurate dosimeters to measure individual blast exposure levels.

fiber degeneration at 2 weeks post-blast (Long et al., 2009). Also using the same shocktube at a higher peak overpressure (241 kPa), with the blast wave focused on the head (inducing 25% mortality), significant multifocal axonal degeneration was observed that was also most prominent at 2 weeks post-blast (Garman et al., 2011). Similarly, axonal degeneration was observed following a range of exposure levels (69–183 kPa) that was prominent at 1–2 weeks post-injury, but was ameliorated by torso shielding (Koliatsos et al., 2011). Combined with our findings, it is possible that axonal degeneration progresses at a slower rate than that observed in non-blast diffuse brain injury, making observations at any single early time-point unimpressive, and suggesting that axonal degeneration is secondary to other primary pathological responses. Alternatively, bTBI may be marked by persistent axonal dysfunction rather than degeneration/disconnection. Regardless, minimum thresholds for perikaryal degeneration appear to be lower than for axonal

degeneration. In addition, we found substantial reactive astrocytosis, most prominently in the cerebellum, but also in the hippocampus, as early as 3 h post-blast. Widespread reactive astrocytosis and inflammation, including microglial activation and neutrophil infiltration, have been observed within hours of blast and persist for days to weeks post-blast (Kaur et al., 1995,1997; Readnower et al., 2010; Saljo et al., 2001). Overall, our findings of stressed/degenerating neurons and reactive astrocytes suggest that these may be sensitive neuropathological markers to establish blast exposure thresholds in parallel with dosimetry calibration.

Due to the complex nature, bTBI is categorized by the mechanism of injury rather than specific pathologies, as follows: Primary bTBI: direct exposure with extremely rapid shifts in air pressure; Secondary bTBI: impacts with shrapnel/munition propelled by explosion (focal, often penetrating injuries); and Tertiary bTBI: acceleration of individual propelled by blast with deceleration due to collision (focal and/or inertial injuries). To focus on the direct blast shockwave effects on the brain, we limited our examination to only primary bTBI, which is thought to be the key mechanism of injury in the majority of mild bTBI cases, and is not confounded by impact or acceleration. Alternate strategies for blast dosimetry include accelerometers and pressure transducers, which are typically heavy and require a power supply. Although these devices may yield a rich, quantitative data set for individual exposure, they will inherently be more expensive and may not be durable in all combat situations, limiting practicality for ubiquitous in-field use. In comparison, there are advantages to our materials-based approach. For instance, our BID requires no external power supply, rendering it low-cost, lightweight, and indefinitely active. Also, the unobtrusive size permits it to be affixed to multiple locations on uniforms and helmets. As such, this technology may provide a lightweight and inexpensive means to assess the effectiveness of blast mitigation strategies by placing BIDs inside and outside of helmets or body armor. Our BID arrays also provide a simple colorimetric read-out. Importantly, our materials-based design can allow for detection of single supra-threshold or cumulative (repeated) blast exposure, thus directing the medical management of the individuals exposed.

Due to the complexity of blast exposure as well as putative ranges in individual tolerances, it is unlikely that a physical dosimeter can accurately detect mild bTBI in all cases. However, this technology can indicate warfighters likely exposed to supra-threshold blast so that they may be removed from harm's way to receive a more thorough evaluation, including an extended neuropsychological examination, and ideally, advanced neuroimaging (Levin et al., 2010; Matthews et al., 2010; Van Boven et al., 2009,) and biomarker analyses (Agoston et al., 2009; Svetlov et al., 2009). Moreover, for suspected bTBI, the diagnosis is complicated due to the common comorbidity of post-traumatic stress disorder (PTSD), which can also manifest with cognitive dysfunction. This underscores the additional interest in developing a blast dosimeter to help distinguish bTBI from PTSD (when not overlapping).

Overall, the BID offers a novel approach for the detection of bTBI. Consideration for future refinements of the BID include enhanced calibration with subtle pathology in a rat model, and initiating more clinically relevant studies using live-fire testing in a large animal model. In particular, the complex neuroanatomy of humans and other larger mammals, denoted by gyrencephalic brains with substantial white matter domains, may be a key feature in the development of blast-induced neuropathology, making rodent models unsuitable for mimicking all aspects of clinical bTBI. Furthermore, the consistency of BID responses following exposure at various orientations to the blast source (orthogonal versus parallel or oblique) will need to be established.

Exposure to blast is evident in extreme cases; however, mild bTBI may occur following lower-magnitude blast exposure not associated with acceleration, impact, or penetrating injuries. In particular, mild bTBI may occur in the absence of overt physical signs following one supra-threshold event or numerous seemingly sub-threshold events. Through early detection of warfighters at risk for sustaining mild bTBI, this technology may improve long-term bTBI outcomes. Future iterations will be tuned to change color following blast exposure at levels inducing subtle brain pathology undetectable by conventional imaging modalities in humans. Such mild TBI can be difficult to diagnose, but has been associated with long-term cognitive and psychological changes, decreased injury thresholds, and increased chances of developing neurodegenerative disorders. In addition, this approach provides a platform to collect blast exposure data in the field, thus improving our understanding of the mechanisms of injury, while establishing and refining minimum exposure thresholds inducing closed-head mild bTBI in humans. This technology also provides a simple yet sensitive measure to assess the performance of blast-mitigation strategies, such as designs for helmets, body armor, and vehicles, by measuring the local blast characteristics relative to exposure thresholds.

Acknowledgments

This work was supported by the Nanotechnology Institute of Philadelphia Proof-of-Concept (PoC) Fund, the Office of Naval Research (ONR) (grant #N00014-05-0303), the Air Force Office of Scientific Research (AFOSR) (grant #FA9550-06-1-0228), and the National Institutes of Health (NIH) (grants #NS038104, #NS056202, and #NS043126). The authors thank Constance J. Mietus and William Lane for technical contributions.

Author Disclosure Statement

No competing financial interests exist.

References

Agoston, D.V., Gyorgy, A., Eidelman, O., and Pollard, H.B. (2009). Proteomic biomarkers for blast neurotrauma: targeting cerebral edema, inflammation, and neuronal death cascades. J. Neurotrauma 26, 901–911.

Campbell, M., Sharp, D.N., Harrison, M.T., Denning, R.G., and Turberfield, A.J (2000). Fabrication of photonic crystals for the visible spectrum by holographic lithography. Nature 404, 53–56.

Cernak, I., Wang, Z., Jiang, J., Bianm X., and Savic, J. (2001). Ultrastructural and functional characteristics of blast injury-induced neurotrauma. J. Trauma 50, 695–706.

Chavko, M., Adeeb, S., Ahlers, S.T., and McCarron, R.M. (2009). Attenuation of pulmonary inflammation after exposure to blast overpressure by N-acetylcysteine amide. Shock 32, 325–331.

Chavko, M., Koller, W.A., Prusaczyk, W.K., and McCarron, R.M. (2007). Measurement of blast wave by a miniature fiber optic

pressure transducer in the rat brain. J. Neurosci. Methods 159, 277–281.

Chavko, M., Prusaczyk, W.K., and McCarron, R.M. (2006). Lung injury and recovery after exposure to blast overpressure. J. Trauma 61, 933–942.

Chavko, M., Prusaczyk, W.K., and McCarron, R.M. (2008). Protection against blast-induced mortality in rats by hemin. J. Trauma 65, 1140–1145; discussion 1145.

Chen, X.H., Meaney, D.F., Xu, B.N., Nonaka, M., McIntosh, T.K., Wolf, J.A., Saatman, K.E., and Smith, D.H. (1999). Evolution of neurofilament subtype accumulation in axons following diffuse brain injury in the pig. J. Neuropathol. Exp. Neurol. 58, 588–596.

Cullen, D,K., Xu, Y., Reneer, D.V., Browne, K.D., Geddes, J.W., Yang, S., and Smith, D.H. (2011). Color changing photonic crystals detect blast exposure. NeuroImage 54 Suppl. 1:, S37–S44.

Dewitt, D.S., and Prough, D.S. (2009). Blast-induced brain injury and posttraumatic hypotension and hypoxemia. J. Neurotrauma. 26, 877–887.

Elder, G.A., and Cristian, A. (2009). Blast-related mild traumatic brain injury: mechanisms of injury and impact on clinical care. Mt. Sinai J. Med. 76, 111–118.

Elsayed, N.M., and Gorbunov, N.V. (2003). Interplay between high energy impulse noise (blast) and antioxidants in the lung. Toxicology 189, 63–74.

Elsayed, N.M., and Gorbunov, N.V. (2007). Pulmonary biochemical and histological alterations after repeated low-level blast overpressure exposures. Toxicol. Sci. 95, 289–296.

Elsayed, N.M., Gorbunov, N.V., and Kagan, V.E. (1997). A proposed biochemical mechanism involving hemoglobin for blast overpressure-induced injury. Toxicology 121, 81–90.

Garman, R.H., Jenkins, L.W., Switzer, R.C. III, Bauman, R.A., Tong, L.C., Swauger, P.V., Parks, S., Ritzel, D.V., Dixon, C.E., Clark, R., Bayir, H., Kagan, V., Jackson, E., and Kochanek, P.M. (2011). Blast exposure in rats with body shielding is characterized by diffuse axonal injury. J. Neurotrauma. 28, 947–959.

Ghiradella, H., Aneshansley, D., Eisner, T., Silberglied, R.E., and Hinton, H.E. (1972). Ultraviolet reflection of a male butterfly: interference color caused by thin-layer elaboration of wing scales. Science 178, 1214–1217.

Gorbunov, N.V., Elsayed, N.M., Kisin, E.R., Kozlov, A.V., and Kagan, V.E. (1997). Air blast-induced pulmonary oxidative stress: interplay among hemoglobin, antioxidants, and lipid peroxidation. Am. J. Physiol. 272, L320–L334.

Hoge, C.W., Goldberg, H.M., and Castro, C.A. (2009). Care of war veterans with mild traumatic brain injury—flawed perspectives. N. Engl. J. Med. 360, 1588–1591.

Hoge, C.W., McGurk, D., Thomas, J.L., Cox, A.L., Engel, C.C., and Castro, C.A. (2008). Mild traumatic brain injury in U.S. Soldiers returning from Iraq. N. Engl. J. Med. 358, 453–463.

Kato, K., Fujimura, M., Nakagawa, A., Saito, A., Ohki, T., Takayama, K., and Tominaga, T. (2007). Pressure-dependent effect of shock waves on rat brain: induction of neuronal apoptosis mediated by a caspase-dependent pathway. J. Neurosurg. 106, 667–676.

Kaur, C., Singh, J., Lim, M.K., Ng, B.L., Yap, E.P., and Ling, E.A. (1995). The response of neurons and microglia to blast injury in the rat brain. Neuropathol. Appl. Neurobiol. 21, 369–377.

Kaur, C., Singh, J., Lim, M.K., Ng, B.L., Yap, E.P., and Ling, E.A. (1997). Ultrastructural changes of macroglial cells in the rat brain following an exposure to a non-penetrative blast. Ann. Acad. Med. Singapore 26, 27–29.

Kinoshita, S., and Yoshioka, S. (2005). Structural colors in nature: the role of regularity and irregularity in the structure. Chemphyschem 6, 1442–1459.

Koliatsos, V.E., Cernak, I., Xu, L., Song, Y., Savonenko, A., Crain, B.J., Eberhart, C.G., Frangakis, C.E., Melnikova, T., Kim, H., and Lee, D. (2011). A mouse model of blast injury to brain: initial pathological, neuropathological, and behavioral characterization. J. Neuropathol. Exper. Neurol. 70, 399–416.

Leung, L.Y., VandeVord, P.J., Dal Cengio, A.L., Bir, C., Yang, K.H., and King, A.I. (2008). Blast related neurotrauma: a review of cellular injury. Mol. Cell Biomech. 5, 155–168.

Levin, H.S., Wilde, E., Troyanskaya, M., Petersen, N.J., Scheibel, R., Newsome, M., Radaideh, M., Wu, T., Yallampalli, R., Chu, Z., and Li, X. (2010). Diffusion tensor imaging of mild to moderate blast-related traumatic brain injury and its sequelae. J. Neurotrauma 27, 683–694.

Li, Y., Lu, Z., Yin, H., Yu, X., Liu, X., and Zi, J. (2005). Structural origin of the brown color of barbules in male peacock tail feathers. Phys. Rev. E Stat. Nonlin. Soft Matter Phys. 72, 010902.

Long, J.B., Bentley, T.L., Wessner, K.A., Cerone, C., Sweeney, S., and Bauman, R.A. (2009). Blast overpressure in rats: recreating a battlefield injury in the laboratory. J. Neurotrauma 26, 827–840.

Martin, E.M., Lu, W.C., Helmick, K., French, L., and Warden, D.L. (2008). Traumatic brain injuries sustained in the Afghanistan and Iraq wars. J. Trauma Nurs. 15, 94–99; quiz 100–101.

Matthews, S.C., Strigo, I.A., Simmons, A.N., O'Connell, R.M., Reinhardt, L.E., and Moseley, S.A. (2011). A multimodal imaging study in U.S. veterans of Operations Iraqi and Enduring Freedom with and without major depression after blast-related concussion. Neuroimage. 54, S69–S75.

Meagher, S., Galifianakis, A., Jannotta, D., Krapiva, P., and Folio, L. (2008). Radiology corner. Answer to last month's radiology case (#29): diffuse axonal injury with negative CT and positive MRI findings. Mil. Med. 173, xx–xxi.

Miklyaev, Y.V., Meisel, D.C., Blanco, A., von Freymann, G., Busch, K., Koch, W., Enkrich, C., Deubel, M., and Wegener, M. (2003). Three-dimensional face-centered-cubic photonic crystal templates by laser holography: fabrication, optical characterization, and band-structure calculations. Applied Physics Letters 82, 1284–1286.

Mittl, R.L., Grossman, R.I., Hiehle, J.F., Hurst, R.W., Kauder, D.R., Gennarelli, T.A., and Alburger, G.W. (1994). Prevalence of MR evidence of diffuse axonal injury in patients with mild head injury and normal head CT findings. AJNR Am. J. Neuroradiol. 15, 1583–1589.

Moochhala, S.M., Md, S., Lu, J., Teng, C.H., and Greengrass, C. (2004). Neuroprotective role of aminoguanidine in behavioral changes after blast injury. J. Trauma 56, 393–403.

Moon, J.H., and Yang, S. (2005). Creating three-dimensional polymeric microstructures by multi-beam interference lithography. J. Macromolecular Science-Polymer Rev. C45, 351–373.

Noh, H., Liew, S.F., Saranathan, V., Prum, R.O., Mochrie, S.G., Dufresne, E.R., and Cao, H. (2010). Double scattering of light from Biophotonic Nanostructures with short-range order. Opt. Express. 18, 11942–11948.

Okie, S. (2005). Traumatic brain injury in the war zone. N. Engl. J. Med. 352, 2043–2047.

Phillips, Y.Y., and Richmond, D.R. (1991). Primary blast injury and basic research: A brief history, in: *Conventional Warfare: Ballistic, Blast, and Burn Injuries*. (R.F. Bellamy, and R. Zajtchuk, eds). Washington, D.C.: Office of the Surgeon General at TMM Publications, pps. 221–240.

Readnower, R.D., Chavko, M., Adeeb, S., Conroy, M.D., Pauly, J.R., McCarron, R.M., and Sullivan, P.G. (2010). Increase in blood-brain barrier permeability, oxidative stress, and activated microglia in a rat model of blast-induced traumatic brain injury. J. Neurosci. Res. 88, 3530–3539.

Risling, M., Plantman, S., Angeria, M., Rostami, E., Bellander, B.M., Kirkegaard, M., Arborelius, U., and Davidsson, J. (2011). Mechanisms of blast induced brain injuries, experimental studies in rats. NeuroImage 54 Suppl. 1, S89–S97.

Saljo, A, Arrhen, F., Bolouri, H., Mayorga, M., and Hamberger, A. (2008). Neuropathology and pressure in the pig brain resulting from low-impulse noise exposure. J. Neurotrauma 25, 1397–1406.

Saljo, A., Bao, F., Haglid, K.G., and Hansson, H.A. (2000). Blast exposure causes redistribution of phosphorylated neurofilament subunits in neurons of the adult rat brain. J. Neurotrauma 17, 719–726.

Saljo, A., Bao, F., Hamberger, A., Haglid, K.G., and Hansson, H.A. (2001). Exposure to short-lasting impulse noise causes microglial and astroglial cell activation in the adult rat brain. Pathophysiology 8, 105–111.

Saljo, A., Bao, F., Jingshan, S., Hamberger, A., Hansson, H.A., and Haglid, K.G. (2002). Exposure to short-lasting impulse noise causes neuronal c-Jun expression and induction of apoptosis in the adult rat brain. J. Neurotrauma 19, 985–991.

Smith, D.H., Chen, X.H., Iwata, A., and Graham, D.I. (2003). Amyloid beta accumulation in axons after traumatic brain injury in humans. J. Neurosurg. 98, 1072–1077.

Smith, D.H., Chen, X.H., Nonaka, M., Trojanowski, J.Q., Lee, V.M., Saatman, K.E., Leoni, M.J., Xu, B.N., Wolf, J.A., and Meaney, D.F. (1999). Accumulation of amyloid beta and tau and the formation of neurofilament inclusions following diffuse brain injury in the pig. J. Neuropathol. Exp. Neurol. 58, 982–992.

Svetlov, S.I., Larner, S.F., Kirk, D.R., Atkinson, J., Hayes, R.L., and Wang, K.K. (2009). Biomarkers of blast-induced neurotrauma: profiling molecular and cellular mechanisms of blast brain injury. J. Neurotrauma 26, 913–921.

Taber, K.H., Warden, D.L., and Hurley, R.A. (2006). Blast-related traumatic brain injury: what is known? J. Neuropsychiatry Clin. Neurosci. 18, 141–145.

Tanielian, T., and Jaycox, L.H. (2008). Invisible wounds of war: psychological and cognitive injuries, their consequences, and services to assist recovery. RAND: Santa Monica, CA.

Van Boven, R.W., Harrington, G.S., Hackney, D.B., Ebel, A., Gauger, G., Bremner, J.D., D'Esposito, M., Detre, J.A., Haacke, E.M., Jack, C.R., Jr., Jagust, W.J., Le Bihan, D., Mathis, C.A., Mueller, S., Mukherjee, P., Schuff, N., Chen, A., and Weiner, M.W. (2009). Advances in neuroimaging of traumatic brain injury and posttraumatic stress disorder. J. Rehabil. Res. Dev. 46, 717–757.

Vukusic, P., and Sambles, J.R. (2003). Photonic structures in biology. Nature 424, 852–855.

Warden, D. (2006). Military TBI during the Iraq and Afghanistan wars. J. Head Trauma Rehabil. 21, 398–402.

Wojcik, B.E., Stein, C.R., Bagg, K., Humphrey, R.J., and Orosco, J. (2010). Traumatic brain injury hospitalizations of U.S. army soldiers deployed to Afghanistan and Iraq. Am. J. Prev. Med. 38, S108–S116.

Xu, Y., Zhu, X., Dan, Y., Moon, J.H., Chen, V.W., Johnson, A.T., Perry, J.W., and Yang, S. (2008). Electrodeposition of three-dimensional titania photonic crystals from holographically patterned microporous polymer templates. Chem. Mat. 20, 1816–1823.

Yang, S., Megens, M., Aizenberg, J., Wiltzius, P., Chaikin, P.M., and Russel, W.B. (2002). Creating periodic three-dimensional structures by multibeam interference of visible laser. Chem. Mat. 14, 2831–2833.

Zi, J., Yu, X., Li, Y., Hu, X., Xu, C., Wang, X., Liu, X., and Fu, R. (2003). Coloration strategies in peacock feathers. Proc. Natl. Acad. Sci. USA 100, 12576–12578.

Address correspondence to:
Douglas H. Smith, M.D.
Center for Brain Injury and Repair
Department of Neurosurgery
University of Pennsylvania
105 Hayden Hall, 3320 Smith Walk
Philadelphia, PA 19104

E-mail: smithdou@mail.med.upenn.edu